AIAA JOURNAL
Vol. 49, No. 7, July 2011

Technical Notes

Aero-Optical Effects of a Directional Infrared Countermeasure Pod in the Transonic Regime

M. A. Richardson,* A. J. Saddington,†
S. A. Ritchie,‡ and K. Knowles§
Cranfield University,
Swindon, England SN6 8LA, United Kingdom
D. H. Titterton¶
Defence Science and Technology Laboratory,
Porton Down, England SP4 0JQ, United Kingdom
and
L. Sjöqvist** and M. Henriksson††
Swedish Defence Research Agency (FOI),
581 11 Linköping, Sweden

DOI: 10.2514/1.J050420

Nomenclature

G = Gladstone–Dale constant
n = refractive index
x = streamwise direction
y = vertical direction
z = direction normal to base of pod
ρ = density

Introduction

DIRECTIONAL infrared countermeasure (DIRCM) systems can use a laser source to disrupt the guidance of an incoming infrared missile. Over the years, there have been significant research and study into the possible disturbances that a laser beam can encounter as it propagates through the atmosphere. When a laser beam crosses a turbulent flow with a variable refractive index, it is subject to phenomena that can degrade its performance, mainly in terms of beam wander and beam distortion. These phenomena can be divided in aero-optical effects [1] and atmospheric propagation problems.

Aims and Objectives

The aim of this project was, therefore, to investigate the possible use of a simple methodology to study laser-beam propagation in a transonic flow and observe the aero-optical effects. The transonic regime was chosen due to its relevance to fast-jet applications and because it adds to the low Mach number data presented recently in the literature [2]. The transonic flow regime has the potential to produce large changes in density and density gradient, which degrade the performance of DIRCM systems, mainly in terms of the variation in the centroid position of the laser beam (beam wander). Laser tests were conducted in a wind tunnel on a half-scale DIRCM pod, and the measured results are compared with a calibrated computational fluid dynamics (CFD) model, which was used to predict the laser path in the turbulent flow in both upstream and downstream directions.

Experimental Setup

The experimental setup consisted of three main parts: the DIRCM pod, the wind tunnel, and the image acquisition system. These are described in more detail in the following subsections.

Directional Infrared Countermeasure Pod

The DIRCM pod under investigation is a 17-sided faceted shape. A half-scale model was manufactured from a solid piece of ureol for use in the wind tunnel. The principal dimensions of the model are shown in Fig. 1. The center of one of the eight sloping facets was fitted with a 10-mm-diam 2-mm-thick glass window mounted flush with the surface of the pod. A Global Laser Technology, Ltd., Sigma laser diode was mounted in the base of the pod, such that the emitted laser light passed through the glass window normal to the faceted surface.

The DIRCM pod and laser assembly were attached to the removable wind-tunnel sidewall in one of two orientations: with the laser pointing upstream 53.1 deg and with the laser pointing downstream 53.1 deg.

Transonic Wind Tunnel

The experiments were conducted in the Shrivenham transonic wind-tunnel facility, which is an intermittent closed-circuit ejector-driven design. The wind-tunnel circuit is orientated in the vertical plane, and a general arrangement is shown in Fig. 2. Sections A to F show the wind-tunnel cross section at various points around the circuit. Section N is the cross section of the nozzle upstream of the working section (also rectangular). Section I is the cross section at the ejector plane downstream of the working section. The working section is 206 mm high and 229 mm wide, with a constant cross-sectional length of 500 mm. A circular window provides optical access to the working section.

The wind tunnel is powered by compressed air, which is supplied by two Howden rotary screw compressors running in series. The compressed air, at 0.7 MPa (gauge), passes through a 4.5 m^3 heat-reactivated desiccant dryer (−21°C dew point) and a 10 μm filter, and then into a 34 m^3 storage tank. The storage tank acts as a heat sink for the compressed air, such that when it is fed into the wind tunnel, it is at approximately ambient temperature. To prevent the wind tunnel from pressurizing, a blowoff box is located just downstream of section D, which allows the wind tunnel to ventilate to atmosphere. The stagnation pressure in the wind tunnel is approximately equal to atmospheric pressure.

The working section Mach number is primarily set by an adjustable nozzle wall, upstream of the test section, and an adjustable diffuser, between the working section and the ejector exit plane. Fine control of the Mach number was achieved by adjustment of the blowing pressure. A computerized feedback control system maintains a constant static pressure in the wind-tunnel contraction and is calibrated against the required test Mach number. A blowing pressure of approximately 0.55 MPa (gauge) was required to maintain a

Received 11 February 2010; revision received 24 January 2011; accepted for publication 3 February 2011.

*Head of Sensors Group.
†Senior Lecturer, Aeromechanical Systems Group.
‡Research Officer, Aeromechanical Systems Group.
§Professor, Head of Aeromechanical Systems Group. Associate Fellow AIAA.
¶Professor and Defence Science and Technology Laboratory Fellow.
**Research Director.
††Research Scientist.

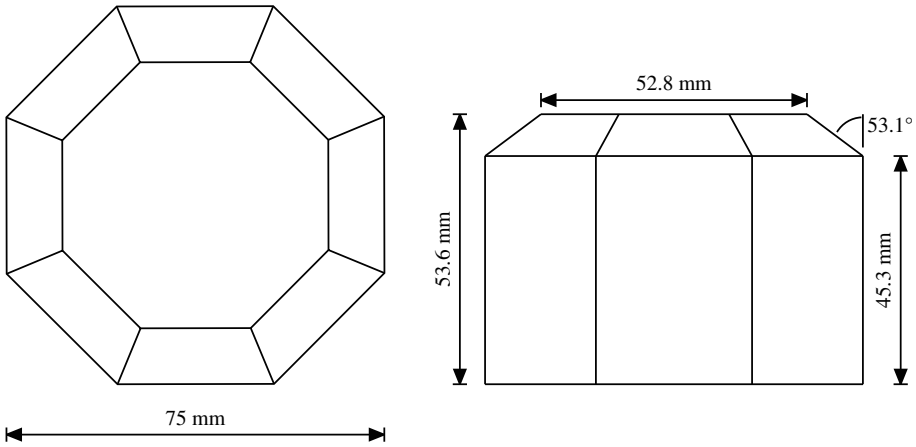

Fig. 1 General arrangement and principal dimensions of the half-scale DIRCM pod.

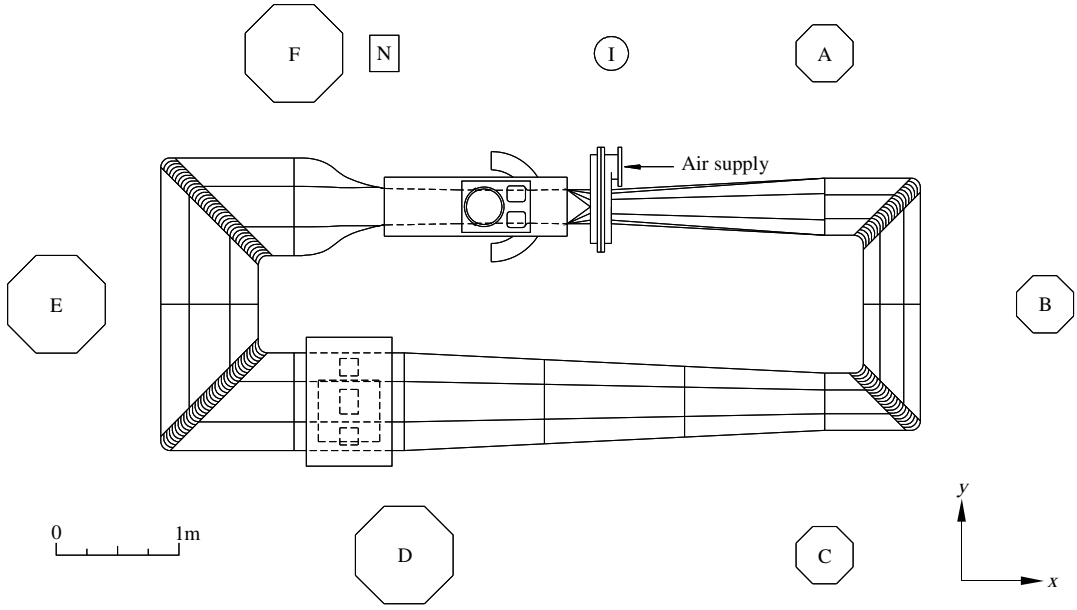

Fig. 2 General arrangement of the Shrivenham transonic wind tunnel.

nominal working section Mach number of 0.73 ± 0.01 with the DIRCM pod installed. The Mach number was determined from pitot static pressure measurements at the entry to the working section. The available data acquisition time during a tunnel run was approximately 10 s. The boundary-layer profile in the wind-tunnel working section at the streamwise position where the DIRCM pod was to be mounted was measured. A profile of total pressure normalized with the freestream value is shown in Fig. 3. The boundary-layer thickness, based on 99% of the freestream total pressure, was 6.4 mm.

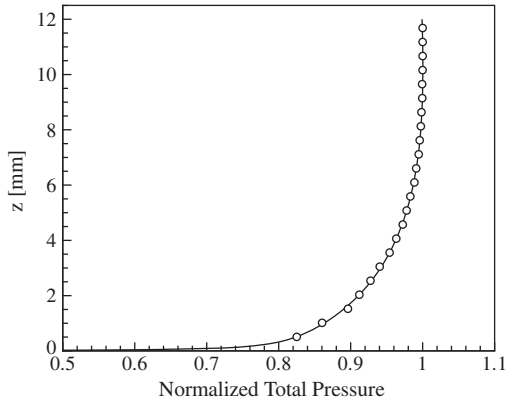

Fig. 3 Boundary-layer profile at streamwise location of DIRCM pod in wind-tunnel test section.

Image Acquisition System

The laser beam propagates through the working section of the wind tunnel and passes through an observation window, constructed from 10-mm-thick optical glass, and onto an observing screen. This is then imaged by a high-speed high-resolution camera system. The camera used in this project was an NAC Image Technology Hi-Dcam II, and it produced audio–video interleave files for subsequent analysis. Data were recorded via a 105 mm focal length lens at 500 Hz, and typically 1638 frames of data were captured. This equates to approximately 3.3 s of data, which was easily obtained within the 10 s of stable run time of the wind tunnel. A MATLAB routine was then used to determine the centroid of the laser beam for each frame. The beam wander in azimuth and elevation was calculated based on the centroid position and the geometry of the experimental setup. The results presented are an average of three runs. The beam wander was shown to be repeatable to within the limits of experimental accuracy, which was determined to be ± 15 μrad.

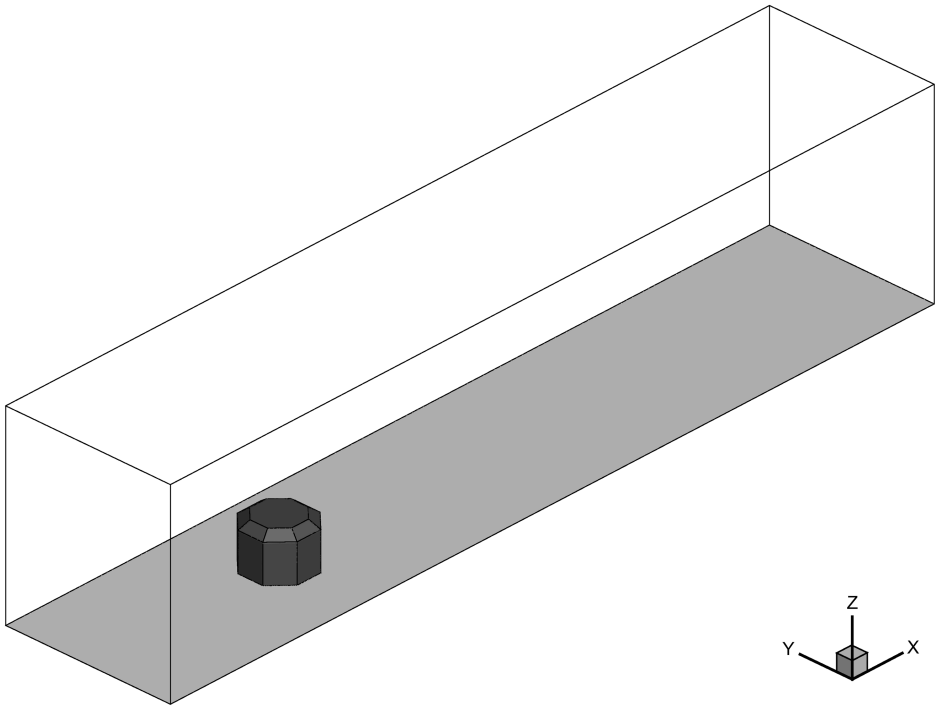

Fig. 4 Computational domain for numerical model of DIRCM pod in wind tunnel.

Numerical Model

A steady-state CFD model of the experiment was developed using a commercial finite volume code. Only a time-averaged laser-beam wander was sought. Hence, a steady-state numerical solution was deemed adequate. The computational domain is shown in Fig. 4. The shaded wall and the pod have no-slip boundary conditions; the remaining three sidewalls have slip boundary conditions. The flow is in the positive x direction. The upstream boundary was positioned such that a turbulent boundary layer of the same thickness as that measured in the wind tunnel would exist in the absence of the DIRCM pod. The downstream boundary of the computational domain was positioned far enough away from the pod to ensure that it had negligible influence on the solution. An unstructured surface mesh was created on the DIRCM pod and the wind-tunnel sidewall to which it was attached. Prismatic cells were grown from these surfaces to form a mesh suitable for near-wall modeling. To reduce computational expense, the other three sides of the wind-tunnel working section were modeled with slip conditions. The remainder of the computational domain was filled with tetrahedral elements. The completed computational model consisted of approximately 1.75 million cells.

The freestream conditions, as determined from experimental measurements, were set to a Mach number of 0.73, a static pressure of 71.085 kPa, and a static temperature of 300 K. The numerical model

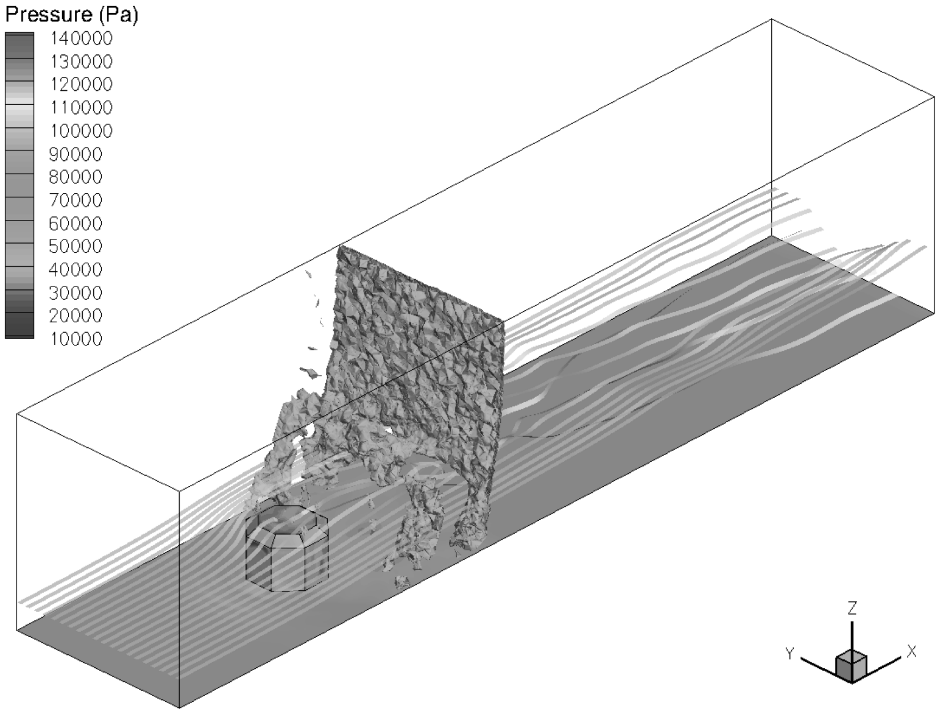

Fig. 5 Some typical results for the numerical model of the DIRCM pod in the wind tunnel.

solved the Navier–Stokes equations in conservative (integral) form. The equations were discretized in space using a second-order-accurate upwind scheme, and a point-implicit linear-equation solver was used in conjunction with an algebraic multigrid method to solve the resultant system of equations. Turbulent calculations were performed using the renormalization group κ-ϵ model [3]. Grid independence was checked by obtaining a solution on a courser, 0.9 million cell, computational mesh; the resulting solution showed negligible difference. Data from the 1.75 million cell mesh were used in later analysis, because they offered better resolution. Solution convergence was determined by monitoring the residuals in the conservation equations and the net mass flux in the domain. The mass flux criteria (the mean net mass flux in the domain should be no greater than $\pm 0.5\%$ of the total) required the greatest number of iterations to satisfy.

Results

Some results from the numerical model are shown in Fig. 5. Contours of static pressure are shown on the pod and surrounding wall; an isosurface identifies a normal shock downstream of the pod. Static pressure contours on the pod are typical of those expected for a bluff body. The numerical model predicted that the blockage caused by the pod results in some local supersonic flow with a consequent normal shock downstream. The normal shock would not, however, be present in the fast-jet installation, because the flow would not be constrained in the same way. We were unable to confirm whether the shock wave was present in the wind-tunnel experiments due to a lack of optical access.

Determination of Local Refractive Index

Using the Gladstone–Dale approximation [4],

$$n \approx 1 + \rho G \tag{1}$$

the local refractive index n of the fluid, through which the laser beam passed, was determined. The Gladstone–Dale constant G was taken to be 0.226×10^{-3} m^3 kg^{-1} based on the laser wavelength of 635 nm, while data for the local air density ρ were determined from the numerical model.

Table 1 Summary of laser-beam wander in azimuth

	Upstream		Downstream	
	Angle, μrad	Direction	Angle, μrad	Direction
Wind off	0.0	N/A	0.0	N/A
Predicted	47.7	Upstream	35.4	Upstream
Measured	79.1	Upstream	125.3	Upstream

Table 2 Summary of laser-beam wander in elevation

	Upstream		Downstream	
	Angle, μrad	Direction	Angle, μrad	Direction
Wind off	0.0	N/A	0.0	N/A
Predicted	0.4	Undetermined	0.4	Undetermined
Measured	45.0	Up	45.0	Up

Determination of Laser-Beam Wander

The local refractive index data were used to calculate the index of refraction boundaries and then used as the input to a simple ray-tracing technique [5] to predict the laser propagation path in both the upstream and downstream directions. The predicted beam wander and the measured beam wander, as determined from the high-speed camera measurements, were compared with the beam path, which results from no aero-optical effects (i.e., no-flow conditions). The results of this comparison are shown schematically in Fig. 6, with the numerical values being given in Tables 1 and 2. "Wind off" indicates conditions without the wind tunnel running. The normal shock predicted by the numerical model is located just downstream of the laser path, which does not pass through it.

The laser beam is predicted and measured to wander into the oncoming flow, i.e., deflect upstream. This is true for both upstream and downstream projections of the beam. The predicted and measured values of beam wander in azimuth are of the same order of magnitude for upstream laser propagation, although the predicted values are somewhat less than the measured quantities. There is better agreement between the two methods in terms of laser propagation in the upstream direction versus the downstream direction, where the measured angular beam wander is approximately 3.5 times greater than the prediction.

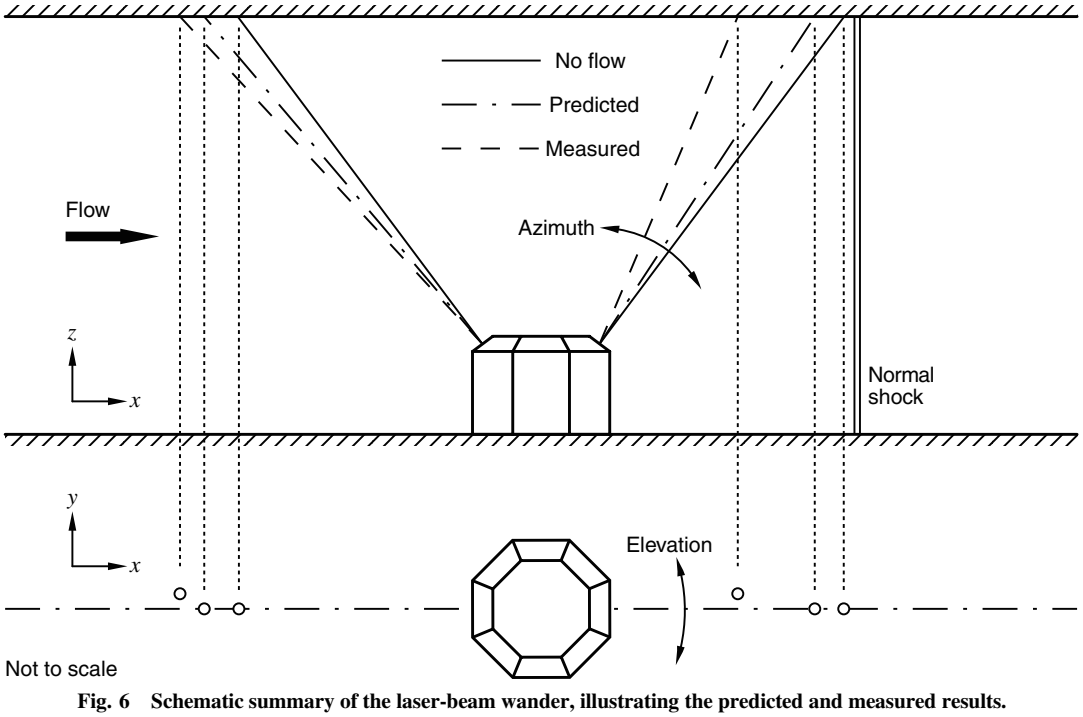

Fig. 6 Schematic summary of the laser-beam wander, illustrating the predicted and measured results.

We identify three main sources of potential discrepancy between the predicted beam wander and the measured values. First, the numerical model is limited in its resolution. The grid resolution varies between 5×10^{-3} mm close to the DIRCM pod and approximately 1.5 mm on the opposite side of the modeled wind tunnel. This was necessary to keep the computational processing time to an acceptable level and, in terms of grid convergence, produced a grid-independent solution. It does, however, mean that the ray-tracing algorithm is working with discrete density changes rather than the continuous changes present in the experiment. An increase in the resolution of the numerical data should improve accuracy. Second, in the experiment, the laser beam as it left the wind tunnel passed through a 10-mm-thick piece of optical glass, and it was not possible to determine the effect this had on the laser path. In the simulation, the laser path did not extend beyond the wind-tunnel wall. Third, the simulation assumes that the inflow conditions to the wind tunnel are symmetrical about the x-z plane. This may not be the case in the experiment and could explain the measured beam wander in elevation, which was not present in the simulation.

Despite the differences between the experimental and numerical predictions, the ray-tracing method presented provides a simple technique for determining laser-beam wander, requiring nothing more than a suitable density field. The technique could be used, therefore, to predict laser-beam wander through any compressible flow phenomenon.

Conclusions

The purpose of this study was to determine if a simple method could be use to predict laser-beam propagation in a transonic flow regime around a DIRCM pod. The experimental process used wind-tunnel measurements to calibrate a CFD model for a specific flow condition. The CFD model was then used to generate flowfield data, and simple calculations were used to convert the local static densities into refractive indices and generate predicted beam wander in the flow conditions. The calculated and measured values of the laser-beam wander were compared. The predicted beam wander results produced azimuth deviations in the same direction and, for upstream propagation, of the same order of magnitude as the measured azimuth deviations.

References

[1] Hugo, R. J., and Jumper, E. J., "Experimental Measurement of a Time-Varying Optical Path Difference by the Small-Aperture Beam Technique," *Applied Optics*, Vol. 35, No. 22, 1996, pp. 4436–4447. doi:10.1364/AO.35.004436

[2] Gordeyev, S., Hayden, T. E., and Jumper, E. J., "Aero-Optical and Flow Measurements Over a Flat-Windowed Turret," *AIAA Journal*, Vol. 45, No. 2, Feb. 2007, pp. 347–357. doi:10.2514/1.24468

[3] Yakhot, A., and Orszag, S. A., "Renormalisation Group Analysis of Turbulence: I. Basic Theory," *Journal of Scientific Computing*, Vol. 1, No. 1, 1986, pp. 1–51. doi:10.1007/BF01061451

[4] Gladstone, J. H., and Dale, T. P., "Researches on the Refraction, Dispersion, and Sensitiveness of Liquids," *Philosophical Transactions of the Royal Society of London*, Vol. 153, No. , 1863, pp. 317–343. doi:10.1098/rstl.1863.0014

[5] Welford, W. T., *Aberrations of Optical Systems*, Taylor and Francis, Washington, D.C., 1986, pp. 45–59.

M. Glauser
Associate Editor